catalysts

MDPI

Article

From PET Bottles Waste to N-Doped Graphene as Sustainable Electrocatalyst Support for Direct Liquid Fuel Cells

Noha A. Elessawy [1], Gordana Backović [2], Janesuda Hirunthanawat [2], Marta Martins [2], Lazar Rakočević [3], Marwa H. Gouda [4], Arafat Toghan [5,6], Mohamed E. Youssef [1], Biljana Šljukić [2] and Diogo M. F. Santos [2,*]

[1] Computer Based Engineering Applications Department, Informatics Research Institute IRI, City of Scientific Research and Technological Applications (SRTA-City), Alexandria 21934, Egypt
[2] Center of Physics and Engineering of Advanced Materials, Laboratory for Physics of Materials and Emerging Technologies, Chemical Engineering Department, Instituto Superior Técnico, Universidade de Lisboa, 1049-001 Lisbon, Portugal
[3] Vinča Institute of Nuclear Sciences-National Institute of the Republic of Serbia, University of Belgrade, Mike Petrovića Alasa 12-14, 11000 Belgrade, Serbia
[4] Polymer Materials Research Department, Advanced Technology and New Materials Research Institute (ATNMRI), City of Scientific Research and Technological Applications City (SRTA-City), Alexandria 21934, Egypt
[5] Chemistry Department, College of Science, Imam Mohammad Ibn Saud Islamic University (IMSIU), Riyadh 11623, Saudi Arabia
[6] Chemistry Department, Faculty of Science, South Valley University, Qena 83523, Egypt
* Correspondence: diogosantos@tecnico.ulisboa.pt

Abstract: Direct liquid fuel cells represent one of the most rapidly emerging energy conversion devices. The main challenge in developing fuel cell devices is finding low-cost and highly active catalysts. In this work, PET bottle waste was transformed into nitrogen-doped graphene (NG) as valuable catalyst support. NG was prepared by a one-pot thermal decomposition process of mineral water waste bottles with urea at 800 °C. Then, NG/Pt electrocatalysts with Pt loadings as low as 0.9 wt.% and 1.8 wt.% were prepared via a simple reduction method in aqueous solution at room temperature. The physical and electrochemical properties of the NG/Pt electrocatalysts are characterized and evaluated for application in direct borohydride peroxide fuel cells (DBPFCs). The results show that NG/Pt catalysts display catalytic activity for borohydride oxidation reaction, particularly the NG/Pt_1, with a number of exchanged electrons of 2.7. Using NG/Pt composite in fuel cells is anticipated to lower prices and boost the usage of electrochemical energy devices. A DBPFC fuel cell using NG/Pt_1 catalyst (1.8 wt.% Pt) in the anode achieved a power density of 75 mW cm^{-2} at 45 °C. The exceptional performance and economic viability become even more evident when expressed as mass-specific power density, reaching a value as high as 15.8 W $mg_{Pt}{}^{-1}$.

Keywords: graphene-based electrocatalyst; PET bottles waste; nitrogen-doped graphene; Pt-based electrocatalyst; borohydride oxidation; direct liquid fuel cells

Citation: Elessawy, N.A.; Backović, G.; Hirunthanawat, J.; Martins, M.; Rakočević, L.; Gouda, M.H.; Toghan, A.; Youssef, M.E.; Šljukić, B.; Santos, D.M.F. From PET Bottles Waste to N-Doped Graphene as Sustainable Electrocatalyst Support for Direct Liquid Fuel Cells. *Catalysts* **2023**, *13*, 525. https://doi.org/10.3390/catal13030525

Academic Editor: David Sebastián

Received: 27 January 2023
Revised: 25 February 2023
Accepted: 1 March 2023
Published: 4 March 2023

1. Introduction

Eco-friendly energy storage and conversion devices are severely needed to solve worldwide energy crises. A fuel cell is a device that converts chemical energy into electricity. Hydrogen is primarilyconsidered to be an energy carrier. In the 1970s, liquid hydrogen was used by NASA as a fuel for space shuttles, and more recently it was employed in fuel cell electric vehicles (FCEVs) [1]. Hydrogen is typically used as compressed gas, which has several issues, such as purification, transportation, and storage, which may lead to safety problems for mobile users. Complex hydrides, such as $NaBH_4$, LiH, and NaH, are known to be capable of storing hydrogen, which makes them a possible alternative to solve this problem.

The direct borohydride peroxide fuel cell (DBPFC) gained significant interest as a strong candidate for different portable applications due to simple liquid fuel handling and its high energy density [2–4]. In particular, DBPFCs present much higher theoretical voltage (E_0 = 3.01 V) than that of the DMFC (E_0 = 1.21 V) and of the H_2-O_2 PEMFC (E_0 = 1.23 V). DBPFC systems have other advantages over conventional hydrogen/oxygen fuel cells, such as long cycle life and environmental safety. Their anode reaction is the direct oxidation of sodium borohydride ($NaBH_4$) in sodium hydroxide (NaOH) solution. Theoretically, the electrooxidation of $NaBH_4$ releases eight electrons, as shown in Equation (1). However, due to the unavoidable hydrolysis of borohydride (BH_4^-) on the electrocatalyst, the number of released electrons is always less than eight [5,6]. The cathodic reaction when hydrogen peroxide is used as an oxidant is provided by Equation (2). Thus, the overall fuel cell reaction occurring in a DBPFC is provided by Equation (3).

$$BH_4^- + 8OH^- \rightarrow BO_2^- + 6H_2O + 8e^- \; E^0 = -1.24 \text{ V vs. SHE}, \quad (1)$$

$$H_2O_2 + 2H^+ + 2e^- \rightarrow 2H_2O \; E^0 = 1.77 \text{ V vs. SHE}, \quad (2)$$

$$NaBH_4 + 4H_2O_2 \rightarrow NaBO_2 + 6H_2O \; E_0 = 3.01 \text{ V}. \quad (3)$$

Achieving a complete eight-electron transfer from BOR is virtually impossible due to the quasi-spontaneous hydrolysis of BH_4^- taking place at the electrode surface, generating hydroxyborohydride (BH_3OH^-). Hence, the actual reaction of BOR is provided by Equation (4), where n refers to the number of exchanged electrons:

$$BH_4^- + nOH^- \rightarrow BO_2^- + (n-2)H_2O + (4-(n/2))H_2 + ne^-. \quad (4)$$

The kinetics and mechanism of borohydride oxidation depend on several variables, such as the concentration of $NaBH_4$ [7], the catalyst materials, and temperature [8]. The borohydride oxidation reaction (BOR) was studied in different materials, including noble and non-noble metals, i.e., platinum (Pt) [9], gold (Au) [10], silver (Ag) [10,11], palladium (Pd) [12], and nickel (Ni) [13]. Au was considered for a long time as the most Faradaic-efficient material for BOR, with the advantage of being simultaneously inactive for the competing BH_4^- hydrolysis reaction, allowing an anodic transfer of close to eight electrons. However, BOR kinetics at Au electrodes are somewhat sluggish. Pd is also electrocatalytically active for both the oxidation of BH_4^- and its intermediates, as well as for H_2 generation/oxidation; however, reaction kinetics are still slower than for Pt [14]. Ni has been reported as a low-cost BOR catalyst ensuring a low (below 0 V vs. RHE) open-circuit potential (OCP) and enabling good net BOR currents [15]. Alloying or mixing different group metals, such as PdNi or CuNi, has increased the activity and selectivity for BOR [16–19].

Among most typical catalysts, Pt is usually the benchmark material for many electrochemical energy conversion and storage applications, including as an electrocatalyst for BOR, owing to its good performance on the fast exchange of between two and four electrons during BH_4^- oxidation [20]. Although it also causes the hydrolysis of BH_4^- [21], many studies have indicated that Pt is one of the most attractive metal catalysts. Along with high performance, Pt comes with a higher price. For this reason, intensive research is underway to develop new highly active catalysts that can use smaller amounts of Pt. Generally, Pt is anchored on low-cost carbon support to reduce the electrocatalyst cost, increase the catalyst surface area, and create abundant active sites that enhance electrocatalyst performance [21–24].

Graphene (G) has proven its efficiency as an excellent 2D support material due to its superior conductivity and unparalleled layers structure with a very high specific surface area and good chemical and thermal stability [25–27]. These qualities led to graphene being used as a support material in energy applications [28,29]. Furthermore, by doping the graphene structure with N atoms, the electron density of the adjacent C atoms is rearranged, prompting an electrophilic center in the neighboring N atoms, and changing the geometry

and enhancing the electron donor character of the prepared nitrogen-doped graphene (NG) [30,31].

The present study has been motivated by the need to develop sustainable carbon-supported electrocatalysts with low cost for fuel cell applications. At the same time, removing non-degradable plastic waste accumulating in the world associated with humankind's excessive plastic use in everyday life is crucial. Considering that plastic is suitable for conversion to carbon material, as it is carbon-rich and the derived carbon contains surface functional groups that enhance its electrochemical performance, efforts are underway toward the valorization of this waste and further use in energy conversion devices [32,33]. Herein, NG is produced by the thermal decomposition of waste PET bottles with urea, and its performance as a stable, high surface area support for Pt nanoparticles is assessed for BOR. The proposed NG synthesis has many advantages over previously followed approaches, including straightforward reaction setup and operational steps, an effective, simple, quick, and environmentally friendly one-pot method that can be easily scaled up, and promising industrial applications. The likelihood of fuel cell commercialization may increase if large-scale, low-cost production is feasible. The electrochemical characterization of the synthesized NG/Pt composite electrocatalysts was performed by cyclic voltammetry (CV) and linear scan voltammetry (LSV), demonstrating the potential application of these materials in DBPFC anodes.

2. Results and Discussion

2.1. Morphological and Structure Characterization of Graphene Doped-N and NG/Pt Catalysts

The surface structure of electrocatalysts greatly influences the catalytic reaction; therefore, the morphology and surface structure of prepared materials were explored using various characteristic tools. From the XRD pattern for prepared NG, NG/Pt_0.5, and NG/Pt_1, as shown in Figure 1a, a slight shifting of the NG/Pt_1 peak corresponding to NG was observed, and that may be due to the introduction of Pt nanoparticles inside NG layers, which alters the interlayer spacing [34]. Moreover, obvious diffraction peaks at 2θ values of 26°, 42.3° and 44.3° are observed, which are indexed to (002), (100), and (101) reflections, respectively, corresponding to the standard C peak (JCPDS No. 75-1621). Additionally, these results indicate that Pt atoms are dispersed uniformly onto NG in the form of small clusters, and no obvious diffraction peaks arising from the possible impurity phases for Pt are observed in X-ray, which may suggest the quantity of Pt used is very small and cannot be detected by XRD [35].

The FTIR spectra of NG, NG/Pt_0.5, and NG/Pt_1 samples are shown in Figure 1b. IR spectra of the three samples exhibit a distinct broad absorption at approximately 3450 cm^{-1} corresponding to the stretching vibration mode of –OH, and the graphitic nature of both samples can be evidenced by the presence of in-plane C=C vibration at 1680 cm^{-1}, which is an intrinsic characteristic of the sp^2 graphitic materials [36–38], and the peak at approximately 1680 cm^{-1} was assigned to the C=O bond. There are no obvious characteristic peaks for Pt.

The adsorption–desorption isotherms of N_2 for synthesized samples appear to be characteristic IUPAC-type IV nature, Figure 1c. A hysteresis loop at relative pressure from 0.4 to 1.0 confirmed the mesoporous structure, while a vertical tail near the relative pressure of 1 witnessed the presence of micropores. Table 1 shows the specific surface area with the mean pore diameter for the prepared samples. The distribution of the average pore sizes observed by the BJH method revealed the highest number of pores of large diameter in the case of NG/Pt_1 (Figure 1d). This, in addition to the largest surface area, can provide a large number of active sites in case of NG/Pt_1 and thus boost its catalytic activity.

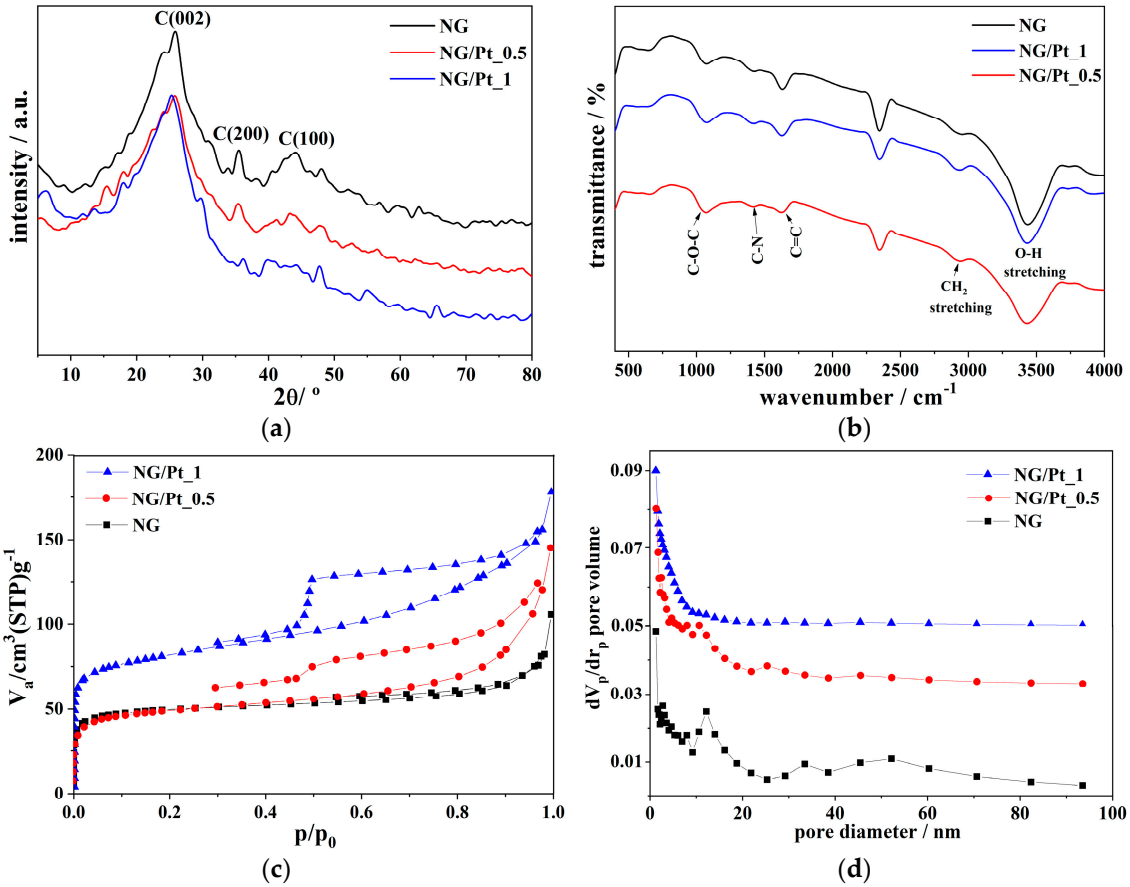

Figure 1. (**a**) XRD patterns, (**b**) FTIR spectra, (**c**) N_2 adsorption–desorption isotherms, and (**d**) average diameter distribution of NG, NG/Pt_0.5, and NG/Pt_1 samples.

Table 1. BET analysis of prepared NG, NG/Pt_0.5, and NG/Pt_1 samples.

	Surface Area (BET) (m^2 g^{-1})	Mean Pore Diameter (nm)
NG	187	3.17
NG/Pt_0.5	181	3.54
NG/Pt_1	303	4.75

The morphology of the as-prepared materials was investigated using transmission electron microscopy (TEM). NG/Pt_1 sample (Figure 2a) shows irregular, non-uniform distributed sheets of NG, while Pt nanoparticles appear as dark spots corresponding to semi-spherical particles packed between the NG layers. The size of Pt nanoparticles ranged between 6.6 and 12.2 nm, with the average size of the Pt nanoparticles of 8.6 nm, as measured from TEM images using ImageJ software. Furthermore, the selected area electron diffraction (SAED) pattern was used for further analysis of NG/Pt_1 sample (Figure 2b). The SAED pattern shows dispersed bright spots and honeycomb rings overlay each other, confirming the multilayered and polycrystalline structure of NG/Pt_1. In addition, a comparably weaker spot of Pt adjoining the carbon lattice is noticeable.

The XPS survey spectra of NG, NG/Pt_0.5, and NG/Pt_1 samples are shown in Figure 3a. The main lines of C 1s, O 1s, and N 1s are clearly visible in all three spectra. Additionally, the Pt 4f line is present in two samples doped with Pt, with the Pt 4f line of the NG/Pt_1 sample having higher intensity as expected. High-resolution spectra of C 1s and N 1s for the NG sample are shown in Figure 3b,c, respectively. C 1s spectra can be deconvoluted into five peaks characteristic of graphene [39]. A narrow peak at 285.1 eV, corresponds to sp^2 hybridized double carbon bond C=C, while a peak at 284.8 eV

corresponds to sp^3 hybridized single carbon bond C-C. The peak at 258.8 eV can be assigned to either C-O or C-N bond or a mixture of both signals. The peak at 286.8 eV originates from the double carbon–oxygen bond C=O, and a final peak at 288.6 eV most probably originates from the O=C-OH bond since the FTIR spectroscopy analyses (Figure 1b) indicate the presence of the –OH group. Peaks corresponding to C-O and C-N bonds are almost at the same position and, therefore, cannot be accurately deconvoluted [40,41]. Relatively low peak intensity of oxygen-containing groups indicates that the graphene is highly reduced. Nitrogen N 1s spectrum is deconvoluted into three peaks. Peaks at 398.6 eV, 399.2 eV, and 400.3 eV correspond to pyridinic, pyrrolic, and graphitic nitrogen groups [40,41].

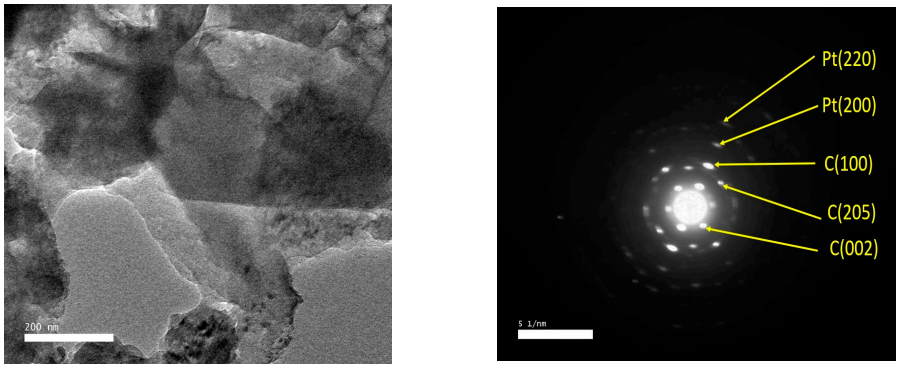

Figure 2. (**a**) TEM image and (**b**) selected area electron diffraction pattern of NG/Pt_1 sample.

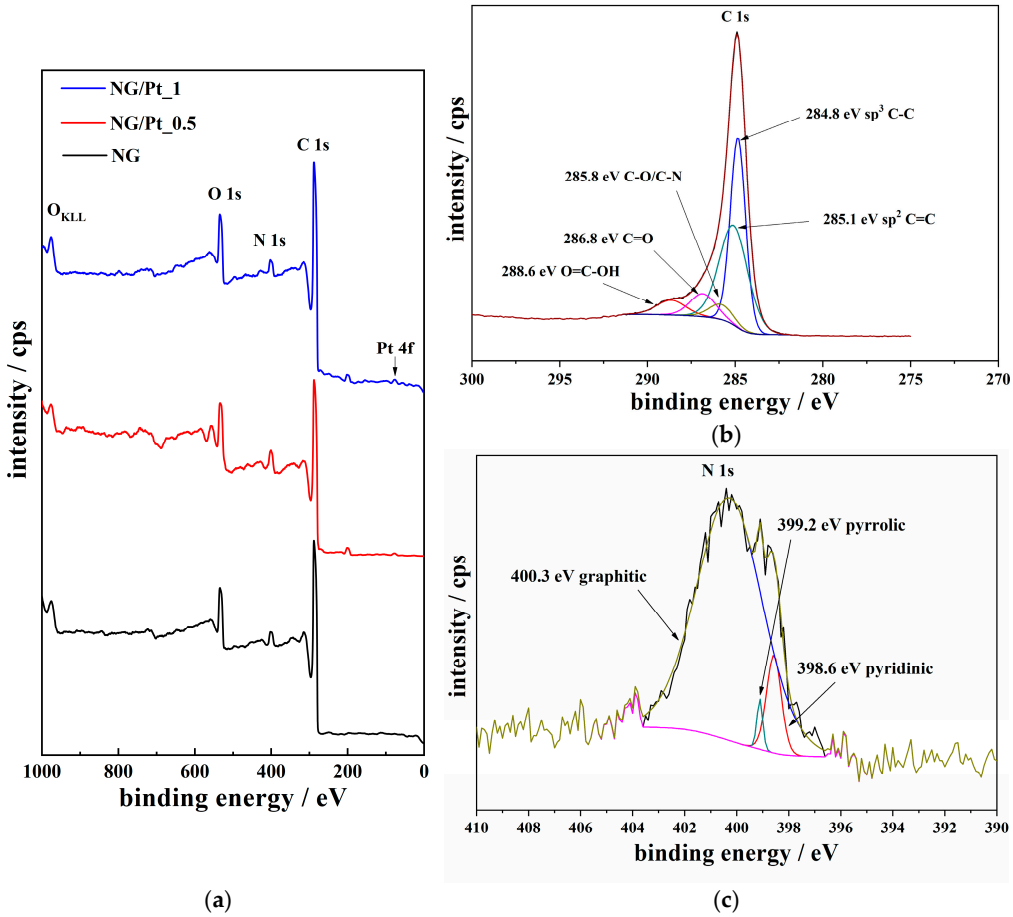

Figure 3. (**a**) XPS survey spectra of NG, NG/Pt_0.5, and NG/Pt_1 samples and high-resolution XPS spectrum of (**b**) C 1s and (**c**) N 1s for NG sample.

The high-resolution spectra of Pt 4f for NG/Pt_0.5 and NG/Pt_1 samples are shown in Figure 4a,b, respectively. For NG/Pt_0.5 sample, the Pt 4f peak contains only one component shown in a typical doublet. The peak at 75.7 eV corresponds to PtO_2 from Pt $4f_{7/2}$, while the peak at 79.8 eV corresponds to PtO_2 from Pt $4f_{5/2}$ [42,43]. Highly upshifted positions of peaks indicate the presence of highly oxidized Pt^{4+}. The peak position shows an even higher upward shift than reported in [43] due to the substrate effect of doped nitrogen into graphene. For NG/Pt_1 sample, Pt 4f line is deconvoluted into two components. The first component at 72.4 eV and 75.9 eV corresponds to PtO from Pt $4f_{7/2}$ and Pt $4f_{5/2}$ peaks, respectively. The second component at 74.7 eV and 77.9 eV corresponds to PtO_2 from Pt $4f_{7/2}$ and Pt $4f_{5/2}$ peaks, respectively [43,44]. Pt present in this sample is slightly less oxidized, showing the presence of both Pt^{2+} and Pt^{4+} species. All four peaks match the positions reported in the literature [43,44], showing only a slight upward shift of less than 0.5 eV in all cases. That indicates a slightly lower impact of the substrate on electron binding energy with an increased amount of Pt.

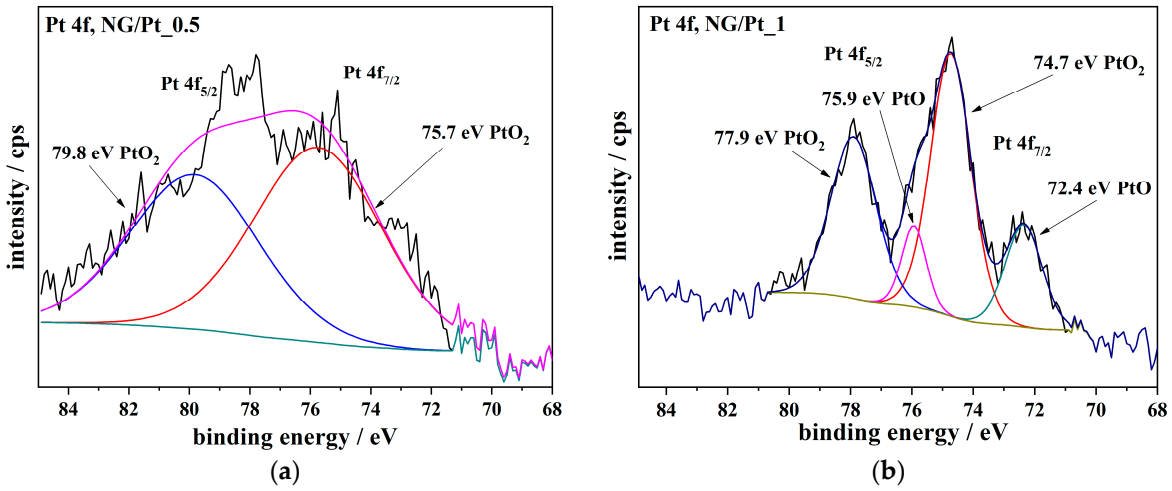

Figure 4. High-resolution XPS spectra of Pt 4f for (**a**) NG/Pt_0.5 and (**b**) NG/Pt_1 samples.

2.2. Electrochemical Measurements

The BOR catalytic performance of the support and the two NG/Pt electrocatalysts prepared was initially investigated by scanning comparative CVs in 2 M NaOH with 0.03 M $NaBH_4$ and in pure 2 M NaOH solution. The CVs of NG/Pt catalysts depicted in Figure 5a,b show the absence of anodic peaks in the BOR potential region in NaOH solution, implying that the current generated during CV measurements run in the presence of BH_4^- originated from its oxidation. Moreover, in the scanned potential range, CVs of NG/Pt catalysts showed one oxidation peak (ca. 0.6 V and 0.7 V for NG/Pt_1 and NG/Pt_0.5, respectively) in the positive scan. An additional sharp oxidation peak was evident in the reverse scan, more pronounced for NG/Pt_1. This peak can be attributed to the oxidation of byproducts originating from the BH_4^- hydrolysis reaction, such as oxidation of adsorbed BH_3OH^- formed during the anodic scan and staying adsorbed on the oxidized electrode surface until being reactivated by reduction in the surface oxides. BH_4^- electrooxidation is a complex reaction with several oxidation peaks: a sharp oxidation peak (a_1) around 0.9 V and a broad oxidation hump (a_2) around 1.4 V on the direct scan, followed by a well-defined oxidation peak at 1.15 V on the reverse scan. Peak a_1 is attributed to the direct oxidation of BH_4^- as an eight-electron process, while wave a_2 and peak c_1 are attributed to the oxidation of BH_3OH^- generated as an intermediate during BH_4^- oxidation. Oxidation peak at reverse scan appears in the potential region where Pt oxides are reduced and the electrode surface is reactivated [45]. Thus, there is a clear competition between the BH_4^- oxidation and its catalytic hydrolysis in the case of NG/Pt anode catalyst, Scheme 1.

H_2 molecules generated during hydrolysis may leave the catalyst's surface or be further oxidized on the same (or another) Pt site [8,10,46].

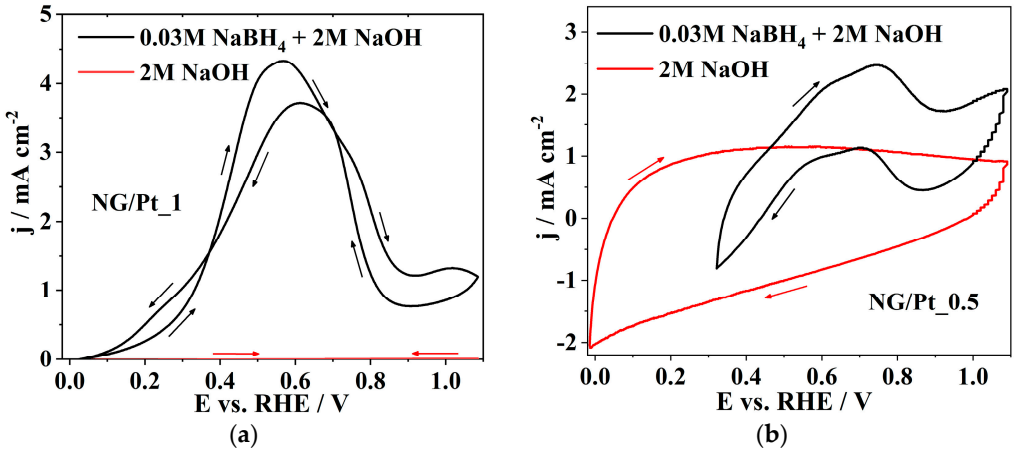

Figure 5. CVs of NG/Pt_1 (**a**) and NG/Pt_0.5 (**b**) in 2 M NaOH solution with and without 0.03 M $NaBH_4$ at 10 mV s^{-1} and room temperature.

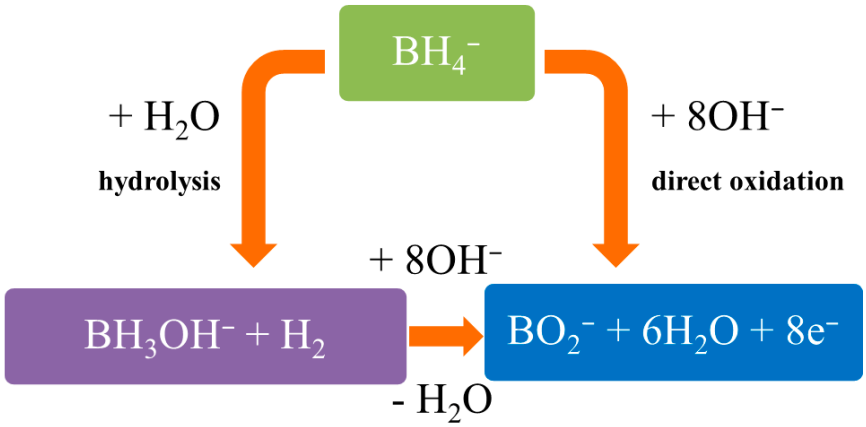

Scheme 1. Schematic illustration of the mechanism of BH_4^- electrooxidation and its hydrolysis as a competing reaction.

NG/Pt_1 exhibited higher BOR catalytic performance, reaching the current density of ca. 4.5 mA cm^{-2}. The enhanced catalytic activity of NG/Pt_1 partially originates from the higher Pt loading. Still, it should be kept in mind that the Pt loading is rather low in the case of both tested electrocatalysts (0.9 wt.% Pt and 1.8 wt.% Pt for NG/Pt_0.5 and NG/Pt_1, respectively). However, as XPS analysis revealed, NG/Pt_1 sample is less oxidized and it is found in both PtO and PtO_2 states. On the other hand, NG/Pt_0.5 sample is more oxidized and is found mostly in PtO_2 state, with Pt in oxidized form being less active for direct BH_4^- oxidation. Moreover, the specific surface area of NG/Pt_1 (303 m^2 g^{-1}) was notably higher than that of NG/Pt_0.5 (181 m^2 g^{-1}), providing a higher number of active sites for BOR to occur. Both features are responsible for a better performance of NG/Pt_1 compared to NG/Pt_0.5, with the latter exhibiting an apparent capacitive behavior in NaOH solution. It should be mentioned that the N-doped graphene support was also tested for BOR but did not show activity.

The reaction kinetics were additionally examined using RDE LSVs (Figure 6). The corresponding j^{-1} vs. $\omega^{-1/2}$ plots for the currents taken at 0.7 V are shown as inset of Figure 6b. From the slope of j^{-1} vs. $\omega^{-1/2}$ plots and using the Koutecky–Levich equation, n values were obtained. n values of 2.7 and 0.7 were obtained for NG/Pt_1 and NG/Pt_0.5,

respectively. The value determined for NG/Pt_1 is comparable with typical n values reported in the literature for BOR at Pt or Pt alloys (two to six electrons) [47].

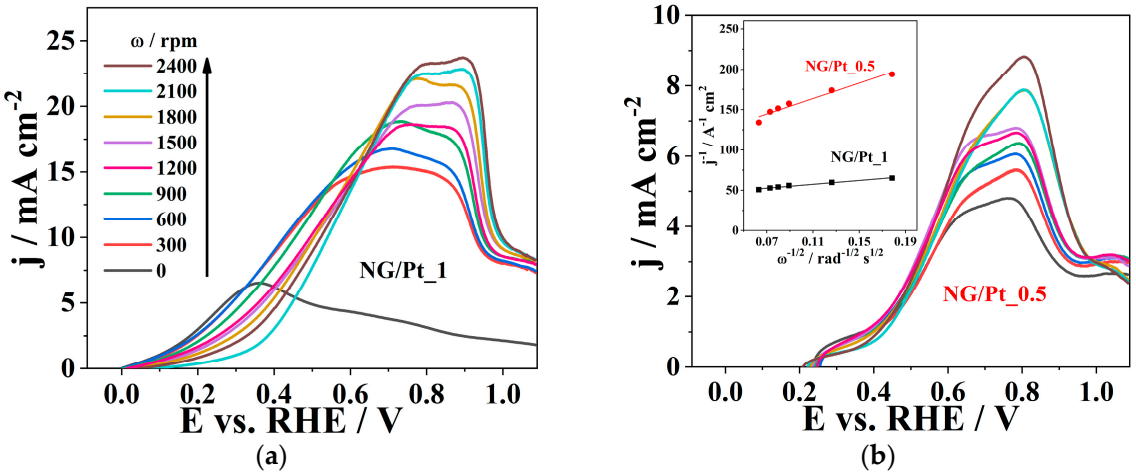

Figure 6. Effect of electrode rotation rate on BOR at NG/Pt_1 (**a**) and NG/Pt_0.5 (**b**) with KL plots in the inset. LSVs run at 10 mV s^{-1} and room temperature.

Poisoning of Pt-based electrocatalysts during BH_4^- oxidation has been reported to be pronounced, especially in BH_4^- solutions of higher concentration [48,49]. Still, no activity loss was observed during BOR experiments within this study. This suggests that using the N-doped graphene support stabilizes Pt nanoparticles, ensuring their uniform distribution throughout the catalyst's operation. The Pt active centers are cleaned of the adsorbed intermediates upon the intermediates' further oxidation.

To evaluate the performance of an NG/Pt_1 anode for a DBPFC, fuel cell tests were performed using a Pt mesh cathode and an NG/Pt_1 anode. Figure 7 depicts the polarization and power density curves of a single cell with NG/Pt_1 anode operating at three different temperatures, 25, 35, and 45 °C.

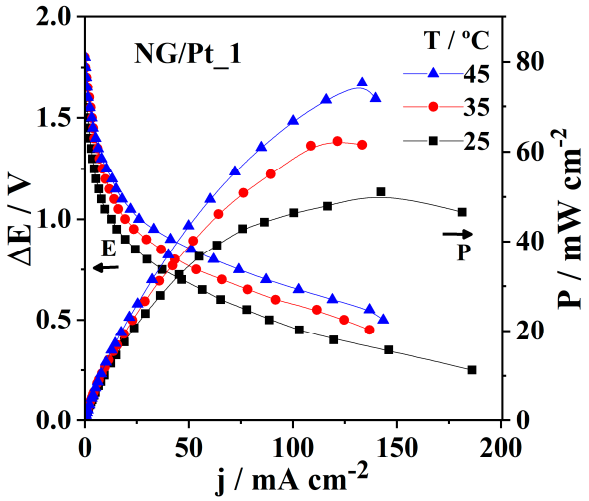

Figure 7. Polarization and power density curves at 25–45 °C for a DBPFC using NG/Pt_1 anode.

As expected, at a higher temperature, the kinetics of the fuel cell reactions were faster, leading to a significant improvement in cell performance. At 45 °C, the power density value reached a maximum of 75 mW cm^{-2} at 1.8 V. The exceptional performance of NG/Pt_1 and great economic viability become even more evident when expressed as mass-specific power density. Namely, a mass-specific peak power density value as

high as 15.8 W mg_{Pt}^{-1} was reached at a cell voltage value of 1.7 V and a current density of 48.2 A mg_{Pt}^{-1}. Obtained DBPFC results were compared with those reported in the literature [49–52]. Table 2 summarizes the DBPFCs results involving Pt and different carbon supports. Notably, the mass-specific performance of DBPFC with NG/Pt_1 clearly surpasses the ones reported in the literature. High mass-specific power density evidences the benefits of using the herein-prepared N-doped graphene as a carbon support that facilitates charge transfer. Its high specific surface area promotes fast charge transfer, enhancing the conductivity path and thus leading to high electrical conductivity [8]. The high specific surface area comes from a higher inter-layer distance (or d-spacing). It has been shown that BOR kinetics and its completion are influenced to a great extent by the mass transport of reactants and intermediates to/from the electrode material's active sites [53,54]. The large pores and layered structure of the herein-prepared NG facilitate both the transport of active species within the electrocatalyst's porous structure to active sites and the escape of generated hydrogen (thus cleaning the active sites from the gas bubbles).

Table 2. Summary of DBPFCs results employing carbon-supported Pt-based electrocatalysts.

Anode	Separator	Fuel	Oxidant	T/°C	P_{max}/W mg_{Pt}^{-1}	j_{max}/ $mAcm^{-2}$	Source
Pt/PPy[2]-$C_{12\%}$ (0.04 mg_{Pt} cm^{-2})	Nafion 117	1 M $NaBH_4$ + 4 M NaOH	5 M H_2O_2 + 1.5 M HCl	RT[1]	0.57	70.3	[8]
Pt/PPy[2]-$C_{20\%}$ (0.04 mg_{Pt} cm^{-2})	Nafion 117	1M $NaBH_4$ + 4 M NaOH	5 M H_2O_2 + 1.5 M HCl	RT[1]	0.75	76.0	[8]
Pt/PPy[2]-$C_{35\%}$ (0.06 mg_{Pt} cm^{-2})	Nafion 117	1 M $NaBH_4$ + 4 M NaOH	5 M H_2O_2 + 1.5 M HCl	RT[1]	0.79	120	[8]
Pt/NPC[3] (4 mg_{Pt} cm^{-2})	Nafion 117	1 M $NaBH_4$ + 3 M NaOH	2 M H_2O_2 + 0.5 M H_2SO_4	RT[1]	0.01	120	[10]
Pt/CB[4] (0.5 mg_{Pt} cm^{-2})	Nafion 117	0.1 M $NaBH_4$ + 6 M NaOH	0.1 M H_2O_2	RT[1]	0.01	18.0	[47]
PtNi/C (1 mg_{PtNi} cm^{-2})	Nafion 117	1 M $NaBH_4$ + 2 M NaOH	2 M H_2O_2 + 0.5 M H_2SO_4	45	0.57	100	[46]
NG/Pt_1 (0.02 mg_{Pt} cm^{-2})	Nafion 117	1 M $NaBH_4$ + 4 M NaOH	5 M H_2O_2 + 1.5 M HCl	45	15.8	137	This study

RT[1]—room temperature; PPy[2]—polypyrrole; NPC[3]—nanoporous carbon; CB[4]—carbon black.

3. Materials and Methods

3.1. Preparation

Nitrogen-doped graphene was synthesized from PET plastic water bottle wastes by pyrolyzing them with urea at 800 °C for 1 h, following a procedure similar to that reported by Elessawy et al. [34]. The final resulting powder was collected and ground as a fine powder. NG/Pt catalysts with metal loadings of 1.8 and 0.9 wt.% Pt were prepared by adding the required amounts of NG powder and chloroplatinic acid solution ($H_2PtCl_6 \cdot 8$ wt.%H_2O) into a beaker under gentle stirring for 1 h. Then, 1 mL of 1 M $NaBH_4$/1 M NaOH solution was added with gentle stirring for 24 h. The resultant catalyst was filtered and rinsed with de-ionized water until no Cl was identified, then dried for 12 h at 60 °C. All chemicals were acquired from Sigma-Aldrich (St. Louis (MO), USA) and used as received, unless otherwise specified.

3.2. Characterization

The basic characterization analysis for prepared catalysts was carried out, including determining the crystal size from XRD (Shimadzu-7000, Kyoto, Japan) with CuKα beam and a scan speed of 4° per min, the surface functional groups by using FTIR spectrophotometer (Shimadzu FTIR-8400S, Kyoto, Japan) with spectra range from 400 to 4000 cm^{-1}. The elemental analysis of prepared catalysts was measured by using EDAX, and morphology was assessed by TEM (JEOL JEM-1230, Tokyo, Japan). The composition of samples was examined by XPS (XP50M X-ray source for Focus 500 and PHOIBOS 100/150 analyzer with AlKα source (1486.74 eV) at a 12.5 kV and 32 mA) and data were analyzed using SPECS Systems (SPECS GmbH, Berlin Germany). The average pore volume and surface area were obtained using BET and BJH adsorption techniques.

3.3. Electrochemical Measurements

The catalytic ink was prepared by ultrasonically dispersing the electrocatalyst (5 mg) into a polyvinylidene difluoride (PVDF) in *N*-methyl pyrrolidone (NMP) solution (5 wt.%,

125 µL) for 30 min. The working electrode was prepared by depositing catalyst ink (3 µL) onto a glassy carbon electrode surface. The working electrode was left in the oven for drying at 75 °C overnight. A typical three-electrode setup was used in the experiment. The platinum coil was used as a counter electrode and a saturated calomel electrode (SCE, Hanna Instruments, Woonsocket (RI), USA) was used as a reference electrode.

To examine the catalysts behavior in 2 M NaOH at room temperature, 2 CVs were recorded in the range from –1.1 V to 0 V at 10 mV s^{-1}. To study the BOR at prepared catalysts at room temperature, 0.03 M of $NaBH_4$ in 2 M NaOH solution was prepared immediately before the measurements. Three cycles were run from the open circuit potential (OCP) to 0 V at 10 mV s^{-1}. Linear scan voltammetry with a rotating disk electrode was run in the range from OCP to 0 V at 10 mV s^{-1} and different rotation rates between 0 and 2400 rpm. Finally, fuel cell tests were conducted under the optimized conditions described in our previous study using 1 M $NaBH_4$ in 4 M NaOH and 5 M H_2O_2 in 1.5 M HCl solutions as an anolyte and catholyte, respectively [51].

4. Conclusions

PET bottle waste was successfully valorized into N-doped graphene as electrocatalyst support. Subsequently, NG/Pt electrocatalysts containing only 0.9 wt.% Pt and 1.8 wt.% Pt were prepared and characterized by XRD, FTIR, XPS, and TEM. N_2-sorption analysis revealed a notably higher specific surface area of NG/Pt_1 that provides a higher number of active sites, thus contributing to its higher activity.

The results obtained from CV and LSV measurements revealed that the catalysts performed well towards BOR. The NG/Pt_1 catalyst exhibited higher activity, evidenced by a number of exchanged electrons of ca. 2.7. Moreover, DBPFC operating at three different temperatures (25, 35, and 45 °C) employing an NG/Pt_1 catalyst showed a maximum power density of 45 mW cm^{-2} at 25 °C, with a significant improvement with a temperature increase and peak power density of 75 mW cm^{-2} at 45 °C. Moreover, a mass-specific power density as high as 15.8 W $mg_{Pt}{}^{-1}$ was reached. Considering the economic aspects of these catalysts and the obtained results, it can be concluded that NG/Pt catalysts are very promising materials for application as anode catalysts in DBPFCs.

Author Contributions: Conceptualization, N.A.E. and D.M.F.S.; methodology, N.A.E., B.Š. and D.M.F.S.; validation, A.T., B.Š. and D.M.F.S.; formal analysis, G.B., M.M.; investigation, N.A.E., G.B., J.H. and L.R.; writing—original draft preparation, N.A.E., M.H.G. and D.M.F.S.; writing—review and editing, M.M., B.Š. and D.M.F.S.; visualization, M.E.Y., A.T. and D.M.F.S.; supervision, B.Š., D.M.F.S.; project administration, N.A.E., M.H.G., M.E.Y. and D.M.F.S. All authors have read and agreed to the published version of the manuscript.

Funding: This research was funded by Fundação para a Ciência e a Tecnologia (FCT, Portugal) through project EXPL/EQU-EQU/0517/2021. FCT also funded a research contract in the scope of programmatic funding UIDP/04540/2020 (D.M.F. Santos) and contract no. IST-ID/156-2018 (B. Šljukić). Thanks to Academy of Scientific Research and Technology and Bibliotheca Alexandria (ASRT-BA) for supporting this research through post-doctoral research; grant project No. 1436.

Data Availability Statement: The data presented in this study are available on request from the corresponding author.

Acknowledgments: Thanks to IAESTE program for supporting the internship of J. Hirunthanawat.

Conflicts of Interest: The authors declare no conflict of interest.

References

1. Sloop, J.L. *Liquid Hydrogen as a Propulsion Fuel*; The NASA History Series; BASA-SP-4404, TL 785558, Stock Number 033-000–00707-8; NASA: Washington, DC, USA, 1978.
2. Gouda, M.H.; Elessawy, N.A.; Toghan, A. Development of effectively costed and performant novel cation exchange ceramic nanocomposite membrane based sulfonated PVA for direct borohydride fuel cells. *J. Ind. Eng. Chem.* **2021**, *100*, 212–219. [CrossRef]

3. Gouda, M.H.; Elessawy, N.A.; Al-Hussain, S.A.; Toghan, A. Design of promising green cation-exchange-membranes-based sulfonated pva and doped with nano sulfated zirconia for direct borohydride fuel cells. *Polymers* **2021**, *13*, 4205. [CrossRef]
4. Gouda, M.H.; Elessawy, N.A.; Toghan, A. Novel crosslinked sulfonated PVA/PEO doped with phosphated titanium oxide nanotubes as effective green cation exchange membrane for direct borohydride fuel cells. *Polymers* **2021**, *13*, 2050. [CrossRef] [PubMed]
5. Merino-Jimenez, I.; Ponce de Leo, C.; Shah, A.A.; Walsh, F.C. Developments in direct borohydride fuel cells and remaining challenges. *J. Power Sources* **2012**, *219*, 339–357.
6. Merino-Jimenez, I.; Leon, C.P.D.; Walsh, F.C. The effect of surfactants on the kinetics of borohydride oxidation and hydrolysis in the DBFC. *Electrochim. Acta* **2014**, *133*, 539–545. [CrossRef]
7. Olu, P.; Bonnefont, A.; Braesch, G.; Martin, V.; Savinova, E.; Chatenet, M. Influence of the concentration of borohydride towards hydrogen production and escape for borohydride oxidation reaction on Pt and Au electrodes e experimental and modelling insights. *J. Power Sources* **2018**, *375*, 300–309. [CrossRef]
8. Oshchepkov, A.; Bonnefont, A.; Maranzana, G.; Savinova, E.; Chatenet, M. Direct borohydride fuel cells: A selected review of their reaction mechanisms, electrocatalysts, and influence of operating parameters on their performance. *Curr. Opin. Electrochem.* **2022**, *32*, 100883.
9. Yi, L.; Yu, B.; Yi, W.; Zhou, Y.; Ding, R.; Wang, X. Carbon Supported Bimetallic Platinum-Iron Nanocatalysts: Application in Direct Borohydride/Hydrogen Peroxide Fuel Cell. *ACS Sustain. Chem. Eng.* **2018**, *6*, 8142–8149. [CrossRef]
10. Rostamikia, G.; Janik, M.J. Direct borohydride oxidation: Mechanism determination and design of alloy catalysts guided by density functional theory. *Energy Environ. Sci.* **2010**, *3*, 1262–1274.
11. Molina Concha, B.; Chatenet, M. Direct oxidation of sodium borohydride on Pt, Ag and alloyed Pt-Ag electrodes in basic media. Part I: Bulk electrodes. *Electrochim. Acta* **2009**, *54*, 6119–6129. [CrossRef]
12. Cheng, K.; Jiang, J.; Kong, S.; Gao, Y.; Ye, K.; Wang, G.; Zhang, W.; Cao, D. Pd nanoparticles support on rGO-C@TiC coaxial nanowires as a novel 3D electrode for $NaBH_4$ electrooxidation. *Int. J. Hydrogen Energy* **2017**, *42*, 2943–2951. [CrossRef]
13. Oshchepkov, A.; Braesch, G.; Ould-Amara, S.; Rostamikia, G.; Maranzana, G.; Bonnefont, A.; Papaefthimiou, V.; Janik, M.; Chatenet, M.; Savinova, E. Nickel Metal Nanoparticles as Anode Electrocatalysts for Highly Efficient Direct Borohydride Fuel Cells. *ACS Catal.* **2019**, *9*, 8520–8528.
14. Hjelm, R.M.E.; Lafforgue, C.; Atkinson, R.W., III; Garsany, Y.; Stroman, R.O.; Chatenet, M.; Swider-Lyons, K. Impact of the Anode Catalyst Layer Design on the Performance of H_2O_2-Direct Borohydride Fuel Cells. *J. Electrochem. Soc.* **2019**, *166*, F1218. [CrossRef]
15. Oshchepkov, A.G.; Braesch, G.; Rostamikia, G.; Bonnefont, A.; Janik, M.J.; Chatenet, M.; Savinova, E.R. Insights into the borohydride electrooxidation reaction on metallic nickel from operando FTIRS, on-line DEMS and DFT. *Electrochim. Acta* **2021**, *389*, 138721. [CrossRef]
16. Vorms, E.A.; Suprun, E.A.; Nartova, A.V.; Kvon, R.I.; Oshchepkov, A.G. Electrodeposited NiCu nanoparticles for the borohydride oxidation reaction: Effect of Cu on the activity and stability of Ni upon surface oxidation. *Electrochim. Acta* **2022**, *433*, 141196.
17. Saha, S.; Gayen, P.; Wang, Z.; Dixit, R.J.; Sharma, K.; Basu, S.; Ramani, V.K. Development of Bimetallic PdNi Electrocatalysts toward Mitigation of Catalyst Poisoning in Direct Borohydride Fuel Cells. *ACS Catal.* **2021**, *11*, 8417–8430. [CrossRef]
18. Santos, D.M.F.; Eugénio, S.; Cardoso, D.S.P.; Šljukić, B.; Montemor, M.F. Three-dimensional nanostructured Ni-Cu foams for borohydride oxidation. *Russ. J. Phys. Chem. A* **2015**, *89*, 2449–2454. [CrossRef]
19. Jovanović, T.; Milikić, J.; Cvjetićanin, N.; Stojadinović, S.; Šljukić, B. Performance of Au/Ti and Au/TiO_2 nanotube array electrodes for borohydride oxidation and oxygen reduction reaction in alkaline media. *Electroanalysis* **2020**, *32*, 1867–1874. [CrossRef]
20. Milikić, J.; Martins, M.; Dobrota, A.S.; Bozkurt, G.; Soylu, G.S.P.; Yurtcan, A.B.; Skorodumova, N.V.; Pašti, I.A.; Šljukić, B.; Santos, D.M.F. A Pt/MnV_2O_6 nanocomposite for the borohydride oxidation reaction. *J. Energy Chem.* **2021**, *55*, 428–436. [CrossRef]
21. McCrum, I.T.; Janik, M.J. First Principles Simulations of Cyclic Voltammograms on Stepped Pt(553) and Pt(533) Electrode Surfaces. *ChemElectroChem* **2016**, *3*, 1609–1617. [CrossRef]
22. Song, C.; Sun, X.; Ye, K.; Zhu, K.; Cheng, K.; Yan, J.; Cao, D.; Wang, G. Electrocatalytic activity of MnO_2 supported on reduced graphene oxide modified Ni foam for H_2O_2 reduction. *Acta Chim. Sin.* **2017**, *75*, 1003–1009. [CrossRef]
23. Cai, Z.; Wang, G.; Song, C.; Yang, X.; Hu, R.; Ye, K.; Zhu, K.; Cheng, K.; Yan, J.; Cao, D. Preparation of a binder free electrode of NiAg supported on graphite modified A4 paper and its electrochemical performance for H_2O_2 reduction. *Chem. J. Chin. Univ.* **2018**, *39*, 1041–1047.
24. Zhao, J.; Gong, J.; Li, Y.; Cheng, K.; Ye, K.; Zhu, K.; Yan, J.; Cao, D.; Wang, G. Self N-doped porous interconnected carbon nanosheets material for supercapacitors. *Acta Chim. Sin.* **2018**, *76*, 107–112. [CrossRef]
25. He, D.; Tang, H.; Kou, Z.; Pan, M.; Sun, X.; Zhang, J.; Mu, S. Engineered graphene materials: Synthesis and applications for polymer electrolyte membrane fuel cells. *Adv. Mater.* **2017**, *29*, 1601741. [CrossRef] [PubMed]
26. Kou, Z.; Meng, T.; Guo, B.; Amiinu, I.S.; Li, W.; Zhang, J.; Mu, S. A generic conversion strategy: From 2D metal carbides (MxCy) to M-self-doped graphene toward highefficiency energy applications. *Adv. Funct. Mater.* **2017**, *27*, 1604904. [CrossRef]
27. Fang, Y.; Hu, R.; Liu, B.; Zhang, Y.; Zhu, K.; Yan, J.; Ye, K.; Cheng, K.; Wang, G.; Cao, D. MXene-derived TiO_2/reduced graphene oxide composite with an enhanced capacitive capacity for Li-ion and K-ion batteries. *J. Mater. Chem. A* **2019**, *7*, 5363–5372. [CrossRef]

28. Taqi-uddeen Safian, M.; Umar, K.; Mohamad Ibrahim, M.N. Synthesis and scalability of graphene and its derivatives: A journey towards sustainable and commercial material. *J. Clean. Prod.* **2021**, *318*, 128603. [CrossRef]
29. Yaqoob, A.A.; Mohamad Ibrahim, M.N.; Umar, K.; Bhawani, S.A.; Khan, A.; Asiri, A.M.; Rizwan Khan, M.; Azam, M.; Al Ammari, A.M. Cellulose Derived Graphene/Polyaniline Nanocomposite Anode for Energy Generation and Bioremediation of Toxic Metals via Benthic Microbial Fuel Cells. *Polymers* **2021**, *13*, 135. [CrossRef]
30. Wu, G.; Santandreu, A.; Kellogg, W.; Gupta, S.; Ogoke, O.; Zhang, H.; Wang, H.-L.; Dai, L. Carbon nanocomposite catalysts for oxygen reduction and evolution reactions: From nitrogen doping to transition-metal addition. *Nano Energ.* **2016**, *29*, 83–110. [CrossRef]
31. Li, B.; Song, C.; Huang, X.; Ye, K.; Cheng, K.; Zu, K.; Yan, J.; Cao, D.; Wang, G. A novel anode for direct borohydride-hydrogen peroxide fuel cell: Au nanoparticles decorated 3D self-supported reduced graphene oxide foam. *ACS Sustain. Chem. Eng.* **2019**, *7*, 11129–11137. [CrossRef]
32. Chen, Z.; Wei, W.; Ni, B.-J.; Chen, H. Plastic wastes derived carbon materials for green energy and sustainable environmental application. *Environ. Funct. Mater.* **2022**, *1*, 34–48. [CrossRef]
33. Yaqoo, L.; Noor, T.; Iqbal, N. Conversion of Plastic Waste to Carbon-Based Compounds and Application in Energy Storage Devices. *ACS Omega* **2022**, *7*, 13403–13435. [CrossRef] [PubMed]
34. Elessawy, N.A.; El Nady, J.; Wazeer, W. Development of High-Performance Supercapacitor based on a Novel Controllable Green Synthesis for 3D Nitrogen Doped Graphene. *Sci. Rep.* **2019**, *9*, 1129. [CrossRef]
35. Yao, R.; Gu, J.; He, H.; Yu, T. Improved Electrocatalytic Activity and Durability of Pt Nanoparticles Supported on Boron-Doped Carbon Black. *Catalysts* **2020**, *10*, 862. [CrossRef]
36. Elkady, M.; Hamad, H.A.; Essawy, N.E. Modification of optical and electrical properties of nanocrystalline $VO_2.0.5H_2O/ZrV_2O_7$: Influence of Cs, Cr and Ga doping. *J. Mater. Res. Technol.* **2019**, *8*, 1212–1223. [CrossRef]
37. Mohamed, M.; Elessawy, N.; Carrasco-Marínc, F.; Hamad, H.A.F. A novel one-pot facile economic approach for the mass synthesis of exfoliated multilayered nitrogen-doped graphene-like nanosheets: New insights into the mechanistic study. *Phys. Chem. Chem. Phys* **2019**, *21*, 13611. [CrossRef] [PubMed]
38. Mohamed, M.; Carrasco-Marín, F.; Elessawy, N.A.; Hamad, H.A.F. GlucoseDerived NDoped Graphitic Carbon: Facile OnePot Graphitic StructureControlled Chemical Synthesis with Comprehensive Insight into the Controlling Mechanisms. *ChemistrySelect* **2020**, *5*, 14685–14702. [CrossRef]
39. Gouda, M.H.; Elnouby, M.; Aziz, A.; Youssef, M.; Santos, D.M.F.; Elessawy, N.A. Green and low-cost membrane electrode assembly for proton exchange membrane fuel cells: Effect of double-layer electrodes and gas diffusion layer. *Front. Mater.* **2020**, *6*, 337. [CrossRef]
40. Al-Gaashani, R.; Najjar, A.; Zakaria, Y.; Mansour, S.; Atieh, M.A. XPS and structural studies of high-quality graphene oxide and reduced graphene oxide prepared by different chemical oxidation methods. *Ceram. Int.* **2019**, *45*, 14439–14448. [CrossRef]
41. Ariharan, A.; Viswanathan, B.; Nandhakumar, V. Nitrogen Doped Graphene as Potential Material for Hydrogen Storage. *Graphene* **2017**, *6*, 41–60. [CrossRef]
42. Arteaga, G.; Rivera-Gavidia, L.M.; Martínez, S.J.; Rizo, R.; Pastor, E.; García, G. Methanol Oxidation on Graphenic-Supported Platinum Catalysts. *Surfaces* **2019**, *2*, 16–31. [CrossRef]
43. Xin, Y.; Liu, J.-G.; Zhou, Y.; Liu, W.; Gao, J.; Xie, Y.; Yin, Y.; Zou, Z. Preparation and characterization of Pt supported on graphene with enhanced electrocatalytic activity in fuel cell. *J. Power Sources* **2011**, *3*, 1012–1018. [CrossRef]
44. Rakočević, L.; Simatović, I.S.; Maksić, A.; Rajić, V.; Štrbac, S.; Srejić, I. PtAu Nanoparticles Supported by Reduced Graphene Oxide as a Highly Active Catalyst for Hydrogen Evolution. *Catalysts* **2022**, *12*, 43. [CrossRef]
45. Šljukić, B.; Santos, D.M.F. Chapter 10—Direct Borohydride Fuel Cells (DBFCs). In *Direct Liquid Fuel Cells*; Akay, R.G., Yurtcan, A.B., Eds.; Academic Press: New York, NY, USA, 2021; pp. 203–232. [CrossRef]
46. Hjelm, S.R.M.E.; Garsany, Y.; Atkinson, R.W., III; Stroman, R.O.; Swider-Lyons, K.; Lafforgue, C.; Chatenet, M. Sodium Borohydride Oxidation on Pt and/or Pd-Based Electrodes in Hydrogen Peroxide Direct Borohydride Fuel Cells (H_2O_2-DBFCs). *ECS Trans.* **2017**, *80*, 1033–1042. [CrossRef]
47. Šljukić, B.; Milikić, J.; Santos, D.M.F.; Sequeira, C.A.C.; Macciò, D.; Saccone, A. Electrocatalytic performance of Pt-Dy alloys for direct borohydride fuel cells. *J. Power Sources* **2014**, *272*, 335–343. [CrossRef]
48. Braesch, G.; Bonnefont, A.; Martin, V.; Savinova, E.R.; Chatenet, M. Borohydride oxidation reaction mechanisms and poisoning effects on Au, Pt and Pd bulk electrodes: From model (low) to direct borohydride fuel cell operating (high) concentrations. *Electrochimi. Acta* **2018**, *273*, 483–494. [CrossRef]
49. Oliveira, R.C.P.; Milikić, J.; Daş, E.; Yurtcan, A.B.; Santos, D.M.F.; Šljukić, B. Platinum/polypyrrole-carbon electrocatalysts for direct borohydride-peroxide fuel cells. *App. Catal. B* **2018**, *238*, 454–464. [CrossRef]
50. Liu, J.; Wang, H.; Wu, C.; Zhao, Q.; Wang, X.; Yi, L. Preparation and characterization of nanoporous carbon-supported platinum as anode electrocatalyst for direct borohydride fuel cell. *Int. J. Hydrogen Energy.* **2014**, *39*, 6729–6736. [CrossRef]
51. Abdolmaleki, M.; Hosseini, M.G. A development in direct borohydride/hydrogen peroxide fuel cell using nanostructured Ni-Pt/C anode. *Fuel Cells* **2017**, *17*, 321–327. [CrossRef]
52. Sombatmankhong, K. Improved performance and stability of direct borohydride fuel cells (DBFCs) with porous polypyrrole. *J. Porous Mater.* **2015**, *22*, 675–687. [CrossRef]

53. Mohan, V.B.; Jayaraman, K.; Bhattacharyya, D. Brunauer–Emmett–Teller (BET) specific surface area analysis of different graphene materials: A comparison to their structural regularity and electrical properties. *Solid State Commun.* **2020**, *320*, 114004. [CrossRef]
54. Kadioglu, T.; Turkmen, A.C.; Ata, K.C.; Akay, R.G.; Tikiz, I.; Celik, C. Investigation of the performance of a direct borohydride fuel cell with low Pt/C catalyst loading under different operating conditions. *Int. J. Hydrogen Energy* **2020**, *45*, 35006–35012. [CrossRef]